Aalto University

Salami, Dariush; Juvakoski, Anni; Vahala, Riku; Beigl, Michael; Sigg, Stephan

Water quality analysis using mmWave radars

Document Version
Peer-reviewed accepted author manuscript, also known as Final accepted manuscript or Post-print

Water quality analysis using mmWave radars

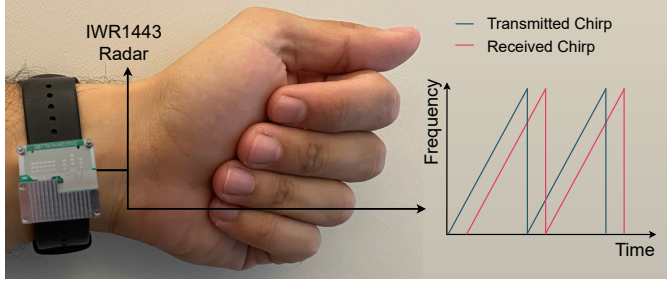Dariush Salami, Anni Juvakoski, Riku Vahala, Michael Beigl, and Stephan Sigg

Fig. 1: An IWR1443 radar installed on a wristband.

Abstract—**Water quality and drinkability assessment are of high importance for various applications from monitoring water utilities to emergency water source evaluation. Traditionally, water quality assessment is done in laboratories with spacious and expensive equipment. We propose a wearable, mmWave Frequency-Modulated Continuous Wave (FMCW) radar based system to assess water quality. Given its small form-factor, low price, and its robustness to lighting and weather conditions, this family of radars can be integrated into wearable devices such as smart-watches, smart glasses, smart rings, etc. Equipped with mmWave radar sensors, such wearables enable seamless monitoring of water quality in hands free settings. The proposed system is able to directly process the In-phase and Quadrature (IQ) data generated by the radar to detect varying levels of different contaminants in four different kinds of water. Specifically, it can identify different concentrations of salt with 100% accuracy, namely nitrate and chloride, as well as detecting different types of waters including Reverse Osmosis (RO), tap, river, and well water with 99.1% accuracy.**

Index Terms—**mmWave radar, AI, ML, water quality analysis**

I. Introduction

Water is a basic requirement for life. Although indiscernible for the naked eye, waters may be polluted with e.g. disease-causing microbes, toxic metals or salt. Probing whether water is suitable for drinking or some other purpose involves laboratory tests, which in turn require special equipment, trained staff, time and materials. In many applications though, analysis of water quality needs to be done relatively fast. Particularly, when the water is in a remote area, it might be infeasible to transport samples for testing. While microbial contamination of water can be mitigated with simple methods such as boiling or filtering, chemical pollution is more difficult

to remove [1]. Therefore, there is an evident need for fast, easy-to-use, and inexpensive testing of chemical constituents in water. Unfortunately, existing water analysis technologies suffer from many problems like only being able to measure a limited number of parameters, large form-factor, and lack of wireless systems [2].

Vast improvements to wearable water quality probing could be brought about by the analysis of reflected electromagnetic radiation in the mmWave spectrum [3]. mmWave radars have been successfully applied to many fields from gesture recognition [4], [5] to localization [6] and glucose level detection [7]. mmWave radars (e.g. IWR1443) feature a small form-factor given their high frequency and are cost efficient. Hence, they are suitable for the integration into wearable devices like smart-watches, smart glasses, smart rings, etc as shown in Fig 1. We propose wearable water quality assessment that is able to overcome the mentioned challenges. We introduce a radar, small enough to be installed in a smart-watch and demonstrate how the radar's contact-less functioning is not hampered by the complexity of water samples. The device is capable of detecting varying levels of different contaminants even in complex water samples, which contain a wide range of other substances. Specifically, it can assess levels of multiple substances at once. We also suggest future applications for this technology. Our main contributions are:

- A novel In-phase and Quadrature (IQ) signal processing pipeline to detect different concentrations of contaminants in different kinds of water samples using mmWave Frequency-Modulated Continuous Wave (FMCW) radars
- An openly available dataset, code [1], and trained models for verification and follow-up research purposes.

II. Related Work

In recent years, radars have been used to assess water quality. Common application cases are remote water quality sensing with devices installed on satellites or airplanes [8]. Further, in-situ radars are installed in liquid tanks or pipes by companies such as Staal instruments and Uponor [2]. In a nutshell, substances and particles in the water cause characteristic refraction in the reflected electromagnetic components. A profile of the water composition can subsequently be established with machine learning [9]. These radars, however, are not portable. A good review of contemporary advancements in portable sensing and bio-sensing used in water quality assessment was recently done [2]. The authors found that these assays are mostly unable to accurately assess complex

D. Salami, and S. Sigg are with communications and networking department and A. Juvakoski, and R. Vahala are with Built Environment department, Aalto University. E-mails: {first_name}.{last_name}@aalto.fi

D. Salami is also with Nokia Bell Labs, Espoo, Finland. dariush.salami@nokia-bell-labs.com

M. Beigl is with the Institute of Telematics, Karlsruhe Institute of Technology (KIT). E-mail : michael@teco.edu

[1]https://version.aalto.fi/gitlab/salamid1/water-quality-with-mmwave-radar
[2]https://bit.ly/3OwI2Dn

(natural) samples. Most of the on-the-go assays are only able to detect a limited number of pollutants, whilst real samples can contain a myriad of diverse compounds. Also, the benefits of portability are often diminished by the lack of a wireless data systems in many assays, although some can be installed on smartphones [2]. Portable solutions usually involve carrying a range of reagents and bulky, yet delicate equipment. They also require training before they may be used reliably.

III. MMWAVE FMCW RADAR PRINCIPLES

FMCW mmWave radars can sense subtle movements due to their high frequency. This leads to a small form-factor. So, this family of radars is becoming increasingly popular. An FMCW radar transmits a sinusoidal signal with increasing frequency sweeping across the whole bandwidth through time (a *chirp*) shown in Fig. 1. A radar *frame* consists of number of chirps. The parameters of the chirp (e.g. slope, chirp duration, bandwidth), determine the performance of the system (e.g. maximum range, range resolution).

A mixer in the processing pipeline of the radar generates an Intermediate Frequency (IF) by subtracting the reflected and transmitted signals. For each reflection, one IF signal is thus generated, which has a constant frequency that is proportional to the round-trip time of the signal component (i.e. the distance to the reflection). Range, velocity, and angle to the target are determined by processing the IF signal. The maximum measurable range is [10]:

$$Range_{max} = \frac{B_{IF} \times c}{2 \times S} \qquad (1)$$

where B_{IF}, c, and S are the maximum IF bandwidth, the speed of light, and the slope of the transmitted chirp, respectively. In this work, an IWR1443 radar is used with a maximum B_{IF} of $15MHz$. Moreover, the maximum Analog to Digital Conversion (ADC) sampling frequency influences B_{IF}. For complex sampling mode $B_{IF} = \frac{0.9 \times ADC_{sampling}}{2}$. To estimate water quality, we choose a short $Range_{max}$ to focus on the sample, suppressing surroundings.

Range resolution is defined as the smallest distance between two separately detectable objects. Based on Eq.2, range resolution only depends on the sweep bandwidth of the chirp [10].

$$Range_{resolution} = \frac{c}{2 \times B} \qquad (2)$$

Here, B is the sweep bandwidth of the FMCW chirp. For the IWR1443 radar, the maximum bandwidth is $4GHz$. This results in a range resolution of approximately $4cm$.

We maximize the the chirp duration to have the maximum ADC samples per chirp. Hence, in our setting, the configuration of the radar is as follows: $77GHz$ start frequency, $3.52MHz/\mu s$ chirp slope, $3Msps$ ADC sampling rate, 2 chirps per frame (with duration $1139\mu s$), $100ms$ frame periodicity, and 2000 frames per recording resulting in 1 sec. total recording per measurement. While this configuration would result in 3374 samples per chirp, the number of samples is constrained by the memory of the radar, so that the actual number of samples is less.

The nature of the reflecting substance (in our case, the water), affects the the received power P_r of the radar:

$$P_r = \frac{P_t G_t G_r \sigma \lambda^2}{(4\pi)^3 R^4}, \qquad (3)$$

where $P_t, G_t, G_r, \sigma, \lambda$, and R are transmit power, transmit antenna gain, receive antenna gain, Radar Cross-Section (RCS), wave-length, and distance from target, respectively. RCS is a measure of how detectable a target is for the radar. It depends on the material, the absolute size, the relative size with respect to the wave-length, the incident and the reflected angles, as well as the polarization of the transmitted and the received signal. Consequently, the material of the target, which is in our case the content of the water, will affect P_r. This will result in different reflection patterns or IQ signal of IF.

IV. MEASUREMENT METHOD

The radar generates IQ data representing the IF signal. The raw data that is captured using a DCA1000 capture card. In particular, the captured data constitutes a 4D tensor of the shape $frames \times chirps \times ADC\_samples \times receive\_antennas$. We process the data directly on the IQ samples. This mitigates the need for pre-processing (e.g. frequency conversion). In addition, we show in Section V that direct IQ sample process is most efficient since it learns better features and achieves higher accuracy.

Since the IQ data has complex entries, the input tensor should be processed using neural networks that support complex weights and activation functions [11]. We utilize a complex-valued 2D-Convolutional Neural Network (CNN) to process the 3D tensors and assume that data from different antennas are independent. Consequently, the input tensor has a shape of $window\_length \times chirps \times ADC\_samples$ where $window\_length$ is a hyperparameter that determines the number of radar frames that should be used to estimate the output of the network. The architecture of the model is shown in Fig. 2. To perform the convolution operation on the complex input, a complex filter matrix $W = A + iB$ with trainable real vectors of A and B is convolved by the complex input vector of $h = x + iy$. Here, x and y are real vectors since the complex signal is represented using real-valued entities. This results in the following convolution operation:

$$W * h = (A * x - B * y) + i(B * x + A * y) \qquad (4)$$

In Eq. 4, to be able to back-propagate gradients to update the weights, the activation and the cost function should be differentiable with respect to the real and imaginary parts of each complex parameter. As shown in Fig. 2, we use an activation function called $cart\_relu$ in the first three layers of the network. This function applies Rectified Linear Unit (ReLU) to both real and imaginary part of the matrix:

$$ReLU(g) = \begin{cases} g & \text{if } g > 0 \\ 0 & \text{otherwise} \end{cases} \qquad (5)$$

$$Cart\_ReLU(z) = ReLU(\Re(z)) + iReLU(\Im(z)) \qquad (6)$$

where $\Re(.)$ and $\Im(.)$ are the real and imaginary parts of the input complex number, respectively. In the *CMaxPoolND*

layer, the only difference between the real and complex-valued parts is the absolute value of the complex input to calculate the element-wise maximum. Finally, the *abs* activation function computes the absolute value of the complex input and returns it. We further propose a second model based on 3D-Complex CNN which accepts a 4D tensor of shape $window\_length \times chirps \times ADC\_samples \times receive\_antenna$. In contrast to the first model, here we assume that the receive antennas are not independent. Hence, we keep them as the last dimension of the input to be processed by a 3D-complex CNN. Equations 4 and 6 still hold for this case. In both models, a *SoftMax* activation function concludes the layers of complex CNN, max pooling, and dense layers to calculate the class probabilities.

V. EVALUATION

We evaluate the system on two settings. First, we identify Reverse Osmosis (RO) water with different levels of contamination including table salt and nitrate. Furthermore, we classify water samples from different sources. We analyze the capabilities of the radar to detect varying concentrations of contaminants (arsenate, fluoride, nitrate and table salt) in four different sample types of RO, tap, well and river water.

A. Experiment Setup

The experiment was designed as if the sensor was integrated into a Smartwatch-like device (see Fig.1): The radar sensor was placed in a similar way as it would have been the case when using a smartwatch, i.e. as if the forearm with the sensor were held over the glass of water. For development purpose, we used an IWR1433 BOOST and a DCA1000 interface board connected to a PC for our experiments (see Fig.3.d).

Different sample concentrations were prepared by adding corresponding masses of table salt (NaCl), potassium nitrate (KNO3, a typical water pollution in farming areas), sodium arsenate (Na3AsO4, a seldom natural poison in water) and sodium fluoride (NaF, an inorganic compound that needed for humans, often used in fluoridation but can be dangerous in heavy doses) to either RO, tap, well or river water. Identical glass beakers were used as sample vessels during measurement. The volume of each sample was 50 ml and the radar was fixed at a distance of $7cm$ from the surface of samples (Fig. 3.d). For each sample, we record 2000 radar frames in 4 trials of 500 frames. The collected data was divided into train (70%), validation (10%), and test 20% sets. An early stopping mechanism with patience of 50 epochs prevents overfitting.

B. Water Contamination Detection

First, we perform salinity level detection. We define seven classes of water for salinity detection: RO water with 0, 10, 20, 30, 40, 50, and $60gr/liter$ of salt. First, we analyze the IF signal for three samples of 0, 30, and $60gr/liter$ in the frequency domain. To visualize the reflection pattern for different salinity levels, the frequencies with Fast Fourier Transform (FFT) magnitude below 10 percent of the magnitude of the dominant FFT component are empirically filtered out. Then, peaks are identified using the Constant False Alarm Rate (CFAR) [12]

TABLE I: Characteristics of water sources. Turbidity and electrical conductivity are shown in Nephelometric Turbidity Unit (NTU) and Millisiemens per Meter (mS/m) units.

feature/water	RO	tap	river	well
pH	5.4	7.9	7.5	6.9
Turbidity	0.08	0.2	6	0.9
EC	0.23	16.1	21.2	18.7

TABLE II: The result for salinity level detection of RO water and the water type detection for five different models. The best Acc., Area Under ROC Curve (AUC), and Average Precision (AP) per row are denoted in bold typeface.

Model	Salinity Level			Water Type		
	Acc.	AUC	AP	Acc.	AUC	AP
SVM	69.2	93.4	69.8	55.4	89.1	50.3
PCA-SVM	64.9	92.1	65.3	50.1	87.3	48.1
FFT-MLP	83.5	98.2	83.7	80.8	97.1	79.3
2D-C-CNN	**100**	**100**	**100**	95.1	99.9	94.8
3D-C-CNN	**100**	**100**	**100**	**99.1**	**100**	**99.5**

algorithm. As shown in Fig. 3, samples from the same salinity level share similar patterns suggesting that the radar can pick up the difference between waters with different levels of salt.

We compared our approach to three other FFT-based models to classify water samples with different levels of salt in Table II. Both proposed models outperform other approaches with an accuracy of 100%. We conclude that end-to-end processing of the IQ signals is more effective than using the signal in the FFT domain.

In the second part of the experiment we trained four binary classifiers on four types of water to identify lower concentrations of table salt, potassium nitrate, sodium arsenate, and sodium fluoride. Since the safety level for arsenate and fluoride is quite low (0.01 and $1.5mg/liter$, respectively), the system could not identify them even the concentration that was 50 times higher than the safety level. For table salt and nitrate, the system was able to achieve an accuracy of 100% for a minimum concentration of $500ml/liter$.

C. Water Type Detection

In this section, we analyze the ability of the models in identifying water from different sources (RO, tap, river, and well water). The characteristics of these waters are shown in Table I. Both proposed methods identify different water sources efficiently with an accuracy of up to 99.1% (TableII). Hence, they are practical for the detection of drinkable water.

VI. CONCLUSION

Here we demonstrate an approach for wearable water quality estimation utilizing miniature mmWave radar devices. Without additional equipment, the radar is capable of detecting even low concentrations of substances like nitrate and salt (NaCl). The system is able to identify contaminant levels above 500 ml/l as well as the source (type) of water. This portable radar, which can be integrated within a smart watch,
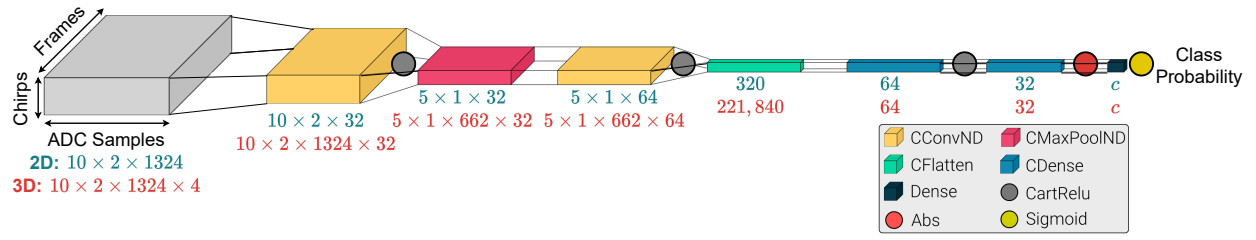
Fig. 2: Proposed model for classifying the samples directly by processing IQ signals
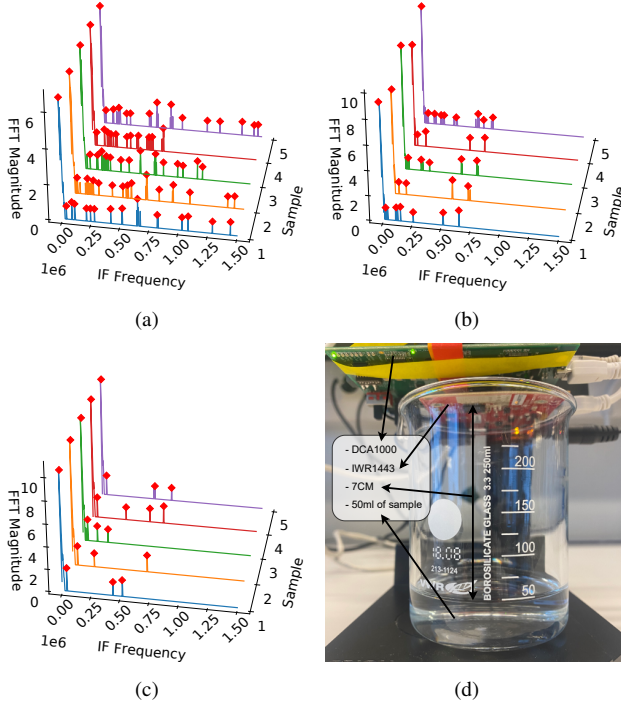

Fig. 3: Peaks in range-FFT after applying CFAR algorithm for random samples of: (a) RO water without salt, (b) RO water with 30 gr/liter of salt (roughly the same salinity as sea water), (c) RO water with 60 gr/liter of salt (d) experimental setup

could have a myriad of applications in various kinds of water and liquid quality testing. An application for the proposed system is liquid quality estimation, i.e. whether it adheres to a trained target profile. This is a necessary daily task in industries dealing with liquids ranging from drink to gasoline production. Tons of resources could be saved if resource-heavy liquid testing could be done in a fraction of time.

Prospectively, the radar may pick up on dangerous concentrations of harmful chemicals to benefit on-the-spot water quality testing. As the detection limit of the radar in $500mg/l$ of a contaminant (at least for nitrate and table salt), it might not be a feasible tool for e.g. detecting if arsenic or fluoride levels are slightly elevated in drinking water. This is because the safety limits of such substances are extremely low [13], [14], [1]. However, the radar is able to detect slightly more prominent changes in water or liquid profiles. Therefore the radar could be trained to aid hikers in assessing whether

water from a stream is drinkable, i.e. if it has a non-complex chemical structure with low concentrations of substances. The radar could also be used for finding sources of pollution in water bodies. Overall, the radar can be used when there is a need to quickly determine whether the quality of a liquid is significantly different compared to a base-line.

In the experiments we used an evaluation board of the radar, as a next step we plan to use the stand-alone radar shown in Fig. 1 and integrate it into a smart-watch. Moreover, we plan to perform more experiments with other types of pollutants.

REFERENCES

[1] F. Edition, "Guidelines for drinking-water quality," *WHO chronicle*, vol. 38, no. 4, pp. 104–108, 2011.
[2] H. Sohrabi *et al.*, "Recent advances on portable sensing and biosensing assays applied for detection of main chemical and biological pollutant agents in water samples: A critical review," *TrAC Trends in Analytical Chemistry*, vol. 143, p. 116344, 2021.
[3] S. Palipana *et al.*, "Pantomime: Mid-air gesture recognition with sparse millimeter-wave radar point clouds," *Proceedings of the ACM on IMWUT*, vol. 5, no. 1, pp. 1–27, 2021.
[4] D. Salami and S. Sigg, "Zero-shot motion pattern recognition from 4d point-clouds," in *IEEE MLSP*. IEEE, 2021, pp. 1–6.
[5] D. Salami *et al.*, "Tesla-rapture: A lightweight gesture recognition system from mmwave radar sparse point clouds," *IEEE TMC*, 2022.
[6] D. Salami, C. J. V. Rubio *et al.*, "User localization using rf sensing: A performance comparison between lis and mmwave radars," in *EUSIPCO*, 2022.
[7] A. E. Omer, S. Safavi-Naeini, R. Hughson, and G. Shaker, "Blood glucose level monitoring using an fmcw millimeter-wave radar sensor," *Remote Sensing*, vol. 12, no. 3, p. 385, 2020.
[8] M. H. Gholizadeh *et al.*, "A comprehensive review on water quality parameters estimation using remote sensing techniques," *Sensors*, vol. 16, no. 8, p. 1298, 2016.
[9] Y. Liang *et al.*, "Fg-liquid: A contact-less fine-grained liquid identifier by pushing the limits of millimeter-wave sensing," *Proceedings of the ACM on IMWUT*, vol. 5, no. 3, pp. 1–27, 2021.
[10] V. Dham, "Programming chirp parameters in ti radar devices," *Application Report SWRA553, Texas Instruments*, 2017.
[11] C. Trabelsi *et al.*, "Deep complex networks," *arXiv preprint arXiv:1705.09792*, 2017.
[12] M. A. Richards, J. A. Scheer, and W. A. Holm, *Principles of Modern Radar: Basic Principles*. Scitech Publishing, 2010.
[13] J. Podgorski and M. Berg, "Global threat of arsenic in groundwater," *Science*, vol. 368, no. 6493, pp. 845–850, 2020.
[14] A. K. Yadav, R. Abbassi, A. Gupta, and M. Dadashzadeh, "Removal of fluoride from aqueous solution and groundwater by wheat straw, sawdust and activated bagasse carbon of sugarcane," *Ecological engineering*, vol. 52, pp. 211–218, 2013.